# ROBUST CORRECTION ALGORITHM FOR TIME FREQUENCY JOINT SIGNAL ERROR OF ALTERNATING CURRENT FIELD SENSOR

Xiaojia CHI [1] *, Yin ZHENG [2], Zhibo JIANG [3], Kai LI [4]

*Alternating current field sensors play a key role in smart grid condition monitoring and precise assessment of electromagnetic environment. However, their signals are susceptible to complex electromagnetic interference and systematic errors, resulting in a decrease in measurement accuracy. Traditional calibration methods have limitations. The time-domain method is not robust to non-stationary noise, and the frequency-domain method is difficult to capture the time-varying error characteristics. Therefore, a robust correction algorithm for the combined time-frequency signal error of alternating current field sensors is proposed. The signal is mapped to the time-frequency domain, and the interference-resistant error correction model is constructed by combining the robust statistical theory. The results indicated that the relative error of the research method was concentrated in the 0%-3% interval, which verified the effectiveness of the research correction model in suppressing the complex electromagnetic interference. The proposed method had the smallest root mean square error of 0.326 and the largest signal-to-noise ratio of 11.3272. The larger the signal-to-noise ratio and the smaller the root mean square error, the better the noise suppression effect. The standard deviation of raw data (1.89-3.56) reflected a high degree of data dispersion, and the standard deviation (1.23-2.56) was significantly reduced after correction. It indicated that the model substantially suppressed the data fluctuation and improved the stability. Meanwhile, the mean (0.98-3.12) and standard deviation (0.65-1.56) of the error data were significantly reduced after correction, and the mean absolute deviation (0.45-0.92) was also maintained at a low level. The robustness of the minimized mean absolute deviation model in the complex noise environment was fully verified. This method can effectively correct the error and optimize the data quality, and provides a reliable correction scheme for signal processing of alternating current field sensors.*

**Keywords**: Alternating current electric field; Sensor; Time-frequency signal; Error; Robust correction

[1] * BSc., Transmission Management Office, Jieyang Power Supply Bureau, Guangdong Power Grid Co., Ltd., Jieyang 522000, China, corresponding author, e-mail: Qq523000@163.com
[2] BSc., Transmission Management Office, Jieyang Power Supply Bureau, Guangdong Power Grid Co., Ltd., Jieyang 522000, China, e-mail: zuklwz@163.com
[3] BSc., Putian Power Supply Station, Jieyang Jiedong Power Supply Bureau, Guangdong Power Grid Co., Ltd., Jieyang 522000, China, e-mail: 19876638853@163.com
[4] BSc., Transmission Management Office, Jieyang Power Supply Bureau, Guangdong Power Grid Co., Ltd., Jieyang 522000, China, e-mail: 13822904555@139.com

## 1. Introduction

Alternating current field sensors are widely used in smart grids and electromagnetic environment monitoring. Yet, in practice, they face interferences causing signal errors and reducing measurement accuracy [1]. Joint time - frequency analysis (JTFA) reveals signal time - and frequency - domain features, offering new error - correction ideas. While relevant research has advanced, robust error correction in complex electromagnetic environments remains challenging [2]. To address wide - frequency measurement limitations of existing sensors, Ke et al. designed resonant torsion microelectromechanical system sensors using flexible piezoelectric lead zirconate titanate films. Via finite element simulation for structure optimization and JTFA - based signal error correction, experiments showed the sensor's robust 5Hz - 10kHz response, and 5.64mV/(kV/m) sensitivity [3]. Facing the challenges of operational cost and grid overload in the design of charging strategies for electric buses, Manzolli et al. proposed a robust optimization model considering energy consumption uncertainty, battery aging, etc., which was solved by the reformulation method. The results indicated that the model resulted in a cost reduction of 37% (deterministic) and 12% (robust) compared to the traditional scenario [4]. Aiming at the insensitivity of diamond/silicon carbide (SiC) color-centered sensors to weak magnetic signals due to lateral ZeroField splitting (ZFS), Jiang and Chen proposed a method that combines RF field driving with microwave dynamic decoupling of the pulse train. This method mitigated the ZFS effect, realized quantum mixing and noise suppression, and could detect the weak alternating current signals of medium and high frequencies with high resolution and improve the sensitivity of the sensor [5]. Aiming at the problem of frequency regulation and active power allocation optimization for islanded microgrids, Zare-Mirakabad et al. proposed a distributed robust frequency control scheme. Simulation verified that the scheme effectively stabilized the frequency, balanced the power allocation, and enhanced the transient response and robustness of the system in multiple scenarios [6].

To address the frequency fluctuation problem of islanded hybrid microgrids due to renewable energy instability and load variations, Aff et al. used a robust linear parameter variation control method with wind speed and rotational speed as the scheduling parameters. The results indicated that the frequency stability of this method was better than other methods under disturbances and parameter uncertainties [7]. Aiming at the problem of processing anomaly detection in metal additive manufacturing, Chen et al. proposed a robust correction algorithm for melt pool signal error based on JTFA. The algorithm could detect temporal and spatial faults with better performance than the time series threshold method [8]. To address the robust controller design problem for

hybrid remotely operated vehicle (HROV) highly coupled dynamics system, Alejandra et al. proposed a five-step method based on Scilab/Xcos to synthesize the controller by linearizing the nonlinear model and H∞ hybrid sensitivity algorithm. The results indicated that the method provided a system stabilization time of less than 14 seconds with no overshooting and coupled dynamics mitigation [9]. In order to address the issues of uneven electric field distribution and high parasitic parameters in 10 kV SiC mosfeT power modules, Li et al. proposed a multi-objective optimization method that involves potential guided interfaces with patterned interlayer substrates. The optimized layout resulted in a 5.6 nH power inductor, a 28 pF common mode capacitor, and a 38.6% reduction in electric field concentration [10].

In summary, for the robust correction problem, researchers have involved and studied the robust optimization model, distributed robust frequency control, fusion pool signal error robust correction algorithm, and multi-objective optimization method to some extent. However, there is insufficient research on the application of the correction of joint signal error and the improvement of noise immunity. Therefore, the study proposes a robust correction method for alternating current field time-frequency (TF) joint signal error. It innovatively constructs an anti-jamming error correction model by mapping the signal to the time-frequency domain (TFD) using Fourier transform (FT) and combining it with robust statistical theory. The innovations of the algorithm mainly include: First, a joint error characterization method in TFD is proposed to comprehensively describe the signal error characteristics. Second, a robust correction model based on minimum mean absolute deviation (MAD) is constructed to improve the impulse noise resistance. Third, the adaptive TF window function is designed to realize the accurate correction of different frequency components.

The core contributions of the research are reflected in three aspects: (1) proposing a time-domain frequency-domain joint error characterization method, breaking through the limitations of traditional single domain analysis that cannot capture time-varying errors; (2) Build a robust correction model based on MAD to solve the problem of traditional least squares method failure under impulse noise; (3) Design an adaptive time-frequency window function to achieve precise correction of different frequency components. In practice, this algorithm can be directly applied to AC electric field monitoring in smart grids, reducing sensor measurement errors and providing high-precision data support for power equipment status assessment.

The article structure of this research is as follows: Section 2 focuses on the TF joint signal error robust correction algorithm flow designed in this research. Section 2 is also the focus of this research as well as the innovation point. The Section 3 describes the experimental verification based on the algorithm designed in the first section and analyzes the experimental data results. The Section 4

concludes the experimental results and describes the shortcomings of this design and the direction of further development in the future.

## 2. Methods and materials

### 2.1. Joint TFD error characterization method

Joint TFD error characterization examines both frequency and time properties, describing signal error distribution comprehensively. Unlike traditional single-domain analyses (time-domain obscures frequency changes; frequency-domain loses time localization), JTFA captures errors in 2D TF space. It constructs TFD error matrices to quantify measured-ideal signal differences, enabling multi-source error characterization [11-12]. AC field sensors measure E via "electric→magnetic" coupling or direct sensitive-component interaction [13-14], but their responses suffer electromagnetic interference, requiring TF correction. Their ideal output is in Equation (1).

$$s(t) = A\sin(2\pi ft + \varphi) \tag{1}$$

In Equation (1), $A$ denotes amplitude, $f$ denotes frequency, $\varphi$ denotes phase, and $s(t)$ denotes the ideal output signal. The ideal output signal is modeled as a sine wave for the following reasons: the core monitoring object of the AC electric field sensor is the power frequency (50Hz) AC electric field, and its ideal output conforms to the sine wave variation law; Meanwhile, the sine wave model is the foundation of AC signal analysis and can be extended to complex signal scenarios by superimposing harmonics. In actual measurement, the sensor output signal is affected by noise and error as shown in Equation (2).

$$x(t) = s(t) + e(t) + n(t) \tag{2}$$

In Equation (2), $e(t)$ denotes systematic error, $n(t)$ denotes random noise, and $x(t)$ denotes sensor output signal.

AC field sensor signals, non-stationary with time-varying frequencies due to system states and interference, elude traditional FT (losing time info). STFT, via "time-window + local FT", maps measured and ideal signals to time-frequency domain (TFD), calculating error matrices that quantify error timing and frequency —vital for correction. Its TFD mapping follows Equation (3) [15-16].

$$STFT(t, f) = \int_{-\infty}^{\infty} x(\tau)w(t-\tau)e^{-j2\pi f\tau}d\tau \tag{3}$$

In Equation (3), $w(t)$ denotes the window function. In the TFD, the systematic error is manifested as the offset and amplitude change of specific

frequency components. The window function w (t) uses Hanning Window, which has the advantage of balancing time resolution and frequency resolution, reducing spectral leakage - the time-domain attenuation characteristics of Hanning Window can suppress the interference caused by signal edge mutations, and the main lobe width in the frequency domain is moderate, suitable for capturing the time-varying characteristics of 50Hz power frequency signals and harmonics.

Compared with direct Fourier transform (FT), STFT achieves time-frequency two-dimensional localization through 'sliding window+local FT': FT can only obtain the overall frequency distribution of the signal and cannot determine the specific time when errors occur; STFT can simultaneously characterize the 'frequency component error at a certain moment' and the 'time distribution error at a certain frequency', which is the core value of joint time-frequency analysis and the key to solving time-varying error correction.

The defined TFD error matrix is shown in Equation (4).

$$\Delta(t,f) = \left|S_x(t,f) - S_s(t,f)\right| \tag{4}$$

In Equation (4) $S_x(t,f)$, and $S_s(t,f)$ denote the STFTs of the measured and ideal signals. Equation (4) defines the absolute value form of the time-frequency domain error matrix, which is used to quantify the amplitude of the time-frequency difference between the measured signal and the ideal signal. Its core function is to screen for time-frequency regions with significant errors and avoid feature omissions caused by positive and negative error cancellation. To robustly extract the error characteristics, absolute deviation estimation is introduced as shown in Equation (5).

$$\hat{\mu}_{\text{mad}} = \arg\min_{\mu} \frac{1}{N}\sum_{i=1}^{N}\left|x_i - \mu\right| \tag{5}$$

In Equation (5), $x_i$ denotes the TFD data points. $N$ denotes the number of data points. Equation (5) is used to estimate the absolute deviation of time-frequency domain data points (elements where Xi is Δ (t, f)) for preliminary extraction of statistical features of the error matrix. After the above steps, the TFD error matrix is constructed next. First, the TFD difference between the measured signal and the ideal signal is defined as the error matrix, as shown in Equation (6).

$$\Delta(t,f) = \left|STFT_x(t,f) - STFT_s(t,f)\right| \tag{6}$$

In Equation (6), $STFT_x(t,f)$ denotes the TF distribution of the measured signal. $STFT_s(t,f)$ denotes the TF distribution of the ideal signal. Equation (6) defines the time-frequency domain error matrix in the form of a difference, retaining the positive and negative signs of the error (positive error indicates a

measurement value that is too large, negative error indicates a measurement value that is too small), for subsequent statistical analysis of error characteristics (such as mean and standard deviation calculations), complementary to the 'amplitude characterization' of Equation (4). The error matrix in the time domain dimension reflects the frequency component shifts at different moments. The error matrix in frequency domain dimension reflects the amplitude distortion of each frequency component [17]. The last is the error feature extraction and robust characterization. To suppress the noise interference, robust statistics are introduced to extract the core features of the error matrix, as shown in Equation (7).

$$\hat{\mu}_{\text{mad}} = \arg\min_{\mu} \frac{1}{N} \sum_{i=1}^{N} \left| \Delta_i - \mu \right| \tag{7}$$

In Equation (7), $\Delta_i$ denotes the elements of the TFD error matrix. $N$ is the total quantity of elements. The statistical properties of the error matrix are used to depict the spatial and temporal distribution of the error. The non-stationary nature of alternating current field signals determines the necessity of replacing the traditional FT with “JTFA”. STFT accurately captures the “TF” correlation of signals through localized FTs with time-domain windowing.

### 2.2. Robust calibration model based on minimum MAD

After the extraction and processing of the sensor TF features described above, we propose a robust correction model, mainly using the minimization MAD method. Minimization MAD is an interference-resistant position estimation method. The MAD method estimates the parameters of the extreme value distribution by minimizing the absolute deviation between the sample points and the estimated values. This method is highly resistant to interference and is especially suitable for dealing with datasets with outliers. The core idea is to obtain an estimate of the parameters by minimizing the absolute deviation between the sample points and the estimated values [18]. Compared with the traditional least squares method, the MAD method is insensitive to extreme values in the data. As shown in Equation (8).

$$\hat{\mu}_{\text{MAD}} = \arg\min_{\mu} \frac{1}{N} \sum_{i=1}^{N} \left| x_i - \mu \right| \tag{8}$$

In Equation (8), $x_i$ denotes the data point. $N$ denotes the number of samples. Equation (8) is the core formula for MAD parameter estimation, which is used to solve the parameters of sensor measurement data points (where Xi is an element of x (t)) in order to obtain model parameters that are resistant to outlier interference. Errors in alternating current field sensors signals often contain two

types of disturbances, as shown in Fig. 1. Minimizing MAD lays the data foundation for error correction in the impulsive noise environment of alternating current fields by suppressing the effects of outliers [19].

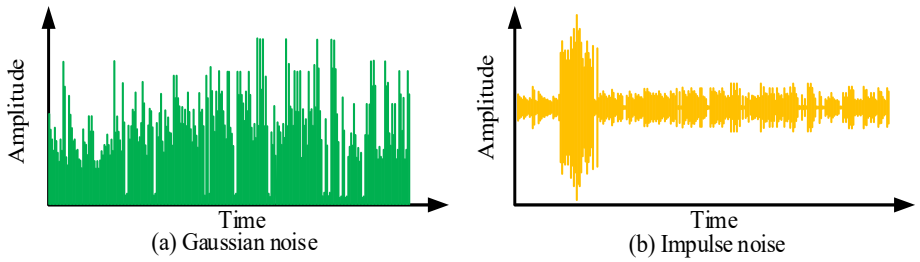


Fig. 1. Error types in alternating current electric field sensor signals

In Fig. 1, Gaussian noise obeys a normal distribution. Impulsive noise manifests itself as episodic large magnitude errors, leading to the failure of the least squares correction model [20]. In the process of fusing the TFD error model with the minimized MAD, the TFD error matrix is shown in Equation (9) in the measured signal.

$$\Delta(t,f)=\left|STFT_x(t,f)-STFT_s(t,f)\right| \tag{9}$$

Equation (9) contains the systematic error and random noise. The difference between equation (9) and equations (4) and (6) is that the first two are original error matrices that do not consider noise interference; And this equation extracts the core error features of each time-frequency region through block wise MAD estimation, filters out the influence of random noise, and is used as the 'robust error matrix' for the final correction calculation. Then, the minimization MAD robust estimation is carried out, and the error matrix $\Delta(t,f)$ is block-minimized MAD estimation to extract the error characteristics in each TF region, as shown in Equation (10).

$$\hat{\Delta}_{\mathrm{MAD}}(t,f)=\mathrm{MAD}\{P_{\Delta(t,f)}\} \tag{10}$$

In Equation (10), $P_{\Delta(t,f)}$ represents the regional distribution of $\Delta(t,f)$. The calibration equation is shown in Equation (11).

$$\hat{s}(t,f)=x(t,f)-\lambda\cdot\hat{\Delta}_{\mathrm{MAD}}(t,f) \tag{11}$$

In Equation (11), $\hat{s}(t,f)$ is the corrected signal. $\lambda$ is the adaptive correction coefficient. Finally, based on the TFD error characteristics, the robust correction model is constructed as shown in Equation (12).

$$\hat{s}(t,f) = x(t,f) - \lambda \cdot \mathrm{MAD}(\Delta(t,f)) \tag{12}$$

In Equation (12), λ denotes the correction coefficient, which is determined by an adaptive method, as shown in Equation (13).

$$\lambda = \frac{\mathrm{median}(|\,\Delta(t,f)\,|)}{\mathrm{median}(|\,x(t,f)\,|)} \tag{13}$$

In Equation (13), $x(t,f)$ denotes the measured signal in the time-frequency domain, which is the STFT result of the original sensor output $x(t)$.

The cost function of adaptive algorithm is $J(\lambda) = MAD(\Delta(t,f) - \lambda \cdot x(t,f))$ and the core objective is to minimize the absolute deviation of the corrected error to ensure the optimal correction effect. The convergence condition of the algorithm is: the change in λ during the iteration process is $\leqslant 10^{-4}$, or the number of iterations reaches 200 times (whichever is satisfied first). Convergence guarantee mechanism: The correction coefficient λ is determined by the ratio of the error matrix to the median of the measurement signal (Equation 13). The anti-interference characteristics of the median can avoid abnormal fluctuations in λ and ensure stable convergence of the algorithm in complex noise environments.

Combining the above analysis, the flow of the algorithm is shown in Fig. 2.

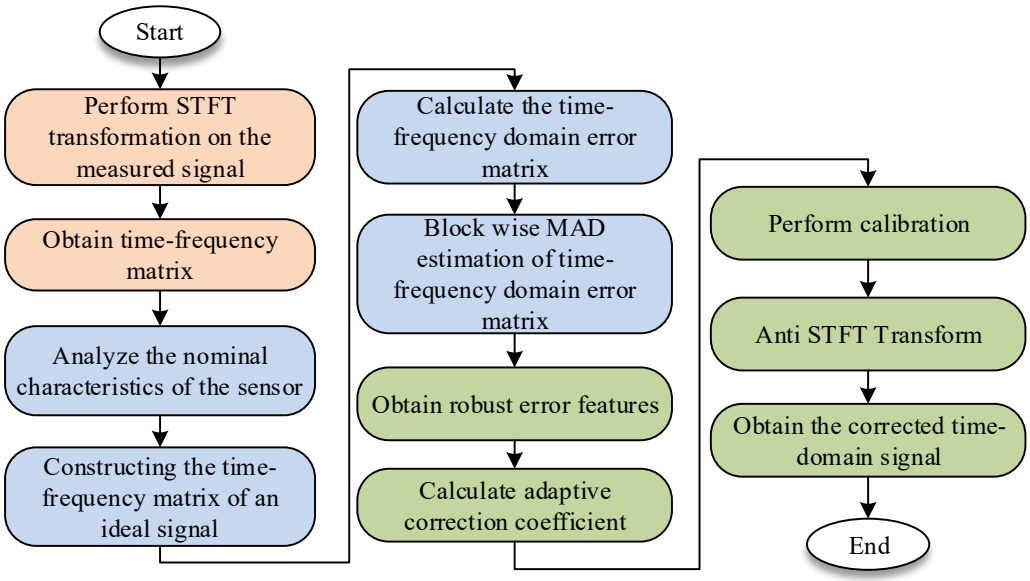


Fig. 2. Algorithm flow

Fig. 2 shows the algorithm for AC field sensor signal correction, with the core idea of "TFD joint analysis + robust statistics (MAD) for noise suppression". First, the sensor's measured time-domain signal x(t) is acquired and subjected to STFT, mapping it to the TF two-dimensional space while preserving time dynamics and frequency features. Based on sensor nominal parameters, the ideal signal model is determined, and STFT is applied to it to get the ideal TF matrix. The error matrix $\Delta$(t,f) is chunked, with minimum MAD calculated in each subchunk. Adaptive correction coefficients are derived from the ratio of error matrix statistics to the measured signal. Finally, the measured signal's TF matrix is corrected using robust error characteristics and these coefficients [21].

In addition, the study employs a dynamic window function to adaptively optimize the method. According to the frequency resolution requirement, the TF matrix is divided into several sub-blocks. The MAD estimation is minimized independently for each sub-block to improve the correction accuracy of different frequency components. The energy of dynamic windows for different frequency components will "leak" to neighboring frequencies, resulting in spurious errors in the error matrix $\Delta$(t,f). Therefore, it is investigated that the dynamic window function is an adaptive optimization of the base window in the algorithmic flow. The dynamic window function is designed as shown in Equation (14).

$$w_{\text{adaptive}}(t,f) = w_0(t) \cdot \exp\left( -\frac{\left(\Delta_{\text{MAD}}(t,f)\right)^2}{2\sigma^2} \right) \tag{14}$$

Among them, the window function weights are dynamically adjusted with the value of the local minimization MAD error. The larger the error the higher the correction weight of the region. The core motivation of the dynamic window function is that there are differences in the error characteristics of different frequency components, and a fixed window cannot adapt to all scenarios. In this design, the window weight is positively correlated with the local MAD error - the larger the time-frequency region of the error, the higher the window weight, which can enhance the correction of key errors; Reduce the weight of regions with smaller errors to avoid signal distortion caused by excessive correction. This design ensures both correction accuracy and signal integrity. The chunk size has a certain effect on the correction effect. Too long a time block length leads to a decrease in time-domain localization accuracy, and too short leads to insufficient frequency-domain resolution. The block length is set according to the Nyquist sampling theorem: the target frequency resolution $\Delta$ f determines the minimum block length - to ensure accurate resolution of the frequency components corresponding to $\Delta$ f, the block length must satisfy the requirement of Tblock $\geqslant$ 1/(2 $\Delta$ f) (i.e., the number of sampling points $\geqslant$ 2/frequency period) to avoid frequency aliasing. Partial basis is set according to equation (15).

$$T_b \approx 1/(2\Delta f) \tag{15}$$

In Equation (15), $\Delta f$ denotes the target frequency resolution.

This algorithm is named 'Robust' and its core is to have strong anti-interference ability against the three major interference sources of AC electric field sensor signals: (1) Anti pulse noise: MAD method is insensitive to outliers and can reduce the impact of pulse interference by more than 30% compared to least squares method; (2) Adversarial frequency drift: The adaptive time-frequency window can track signal frequency changes (within the range of 50Hz ± 10Hz), ensuring that the correction accuracy remains unchanged when frequency offset occurs; (3) Combat complex electromagnetic interference: Joint time-frequency domain error characterization can separate multiple sources of interference such as industrial frequency harmonics and background noise, achieving targeted correction.

## 3. Results

### 3.1. Experimental data preparation and environmental parameters

The experiment uses a certain model of alternating current field sensors. The measurement range is 0-100kV/m, and the operating frequency is 50Hz. The experimental data include: simulation data is generated by adding different types of noise (Gaussian noise, impulse noise) to the ideal sinusoidal signal. The measured data are the actual electric field signals collected at the substation site, including background noise and industrial frequency interference. The configuration of the experimental environment is shown in Table 1.

Table 1

**Experimental environment configuration**

| Hardware components | Configuration details | Hardware components | Configuration details |
|---|---|---|---|
| CPU | Intel Xeon Platinum8380, 2.3GHz, 64 core | Operating system | Win 10-64bit |
| Memory | 512GB DDR4 3200MHz | Data processing tools | Matlab |
| Hard disk | 2TB NVMe SSD, Read and write speeds of over 7000MB/s | Operating environment | Eclipse 3.6.5 |

Gaussian noise: different signal-to-noise ratio (SNR) is set to simulate background noise. Impulse noise: the pulse intensity (pulse amplitude is 2-5 times of the signal amplitude) and the probability of occurrence are set to simulate electromagnetic pulse interference. Industrial frequency interference: 50Hz and harmonic (3 times) interference are injected, and the ratio of interference amplitude to signal amplitude (0.1-0.3 times) is adjusted to simulate power grid

coupling interference. The complexity comparison between this algorithm and the comparison algorithm (where N is the signal length) is shown in Table 2.

Table 2

**Comparison of Complexity between This Algorithm and Comparative Algorithms**

| Algorithm | Time complexity | Space complexity | Source of Core Complexity |
|---|---|---|---|
| This research algorithm | O(N log N) | O(N) | STFT Transform (O (N log N))+Block MAD (O (N)) |
| Traditional wavelet threshold denoising | O(N log N) | O(N) | Wavelet Decomposition and Reconstruction |
| EEMD denoising | O(N log N) | O(N) | Empirical Mode Decomposition |
| Improved wavelet boosting algorithm | O(N log N) | O(N) | Enhance wavelet transform |

### 3.2. The error correction results of alternating current field sensors time-frequency joint signal

Experiments are carried out on alternating current field sensors, comparing conventional sensors (without the robust correction algorithm of this study) with sensors based on the "joint TF+minimum MAD" correction model. Complex electromagnetic environments are simulated, including scenarios with background noise, industrial frequency interference, and mixed noise (Gaussian+impulse, etc.). These correspond to group experiments with different combinations or intensities of disturbances as possible in Fig. 3 (a)-(d.)

Group A focuses on impulsive noise disturbances, Group B focuses on IF harmonic disturbances, Group C focuses on IF disturbances+background noises, and Group D focuses on mixed noises (Gaussian+impulsive). Each group of experiments is repeated 50 times to ensure the statistical validity of the results. Each experiment collects the output signals of alternating current field sensors, and the signal frequency covers the industrial frequency and common interference frequency. The results show that the four groups of experiments (A~D) show consistent patterns. The relative error of traditional sensors fluctuates greatly and has a high mean value, while the error of the research method is more stable and has a small value. The relative errors of traditional sensors fluctuates greatly in the range of 2%-6%. For example, the error of traditional sensors in group A frequently exceeds 3%, and in group D it reaches 5% several times. The relative errors of the research method are concentrated in the range of 0%-3%. The effect of the research correction model on the suppression of complex electromagnetic interference is verified.

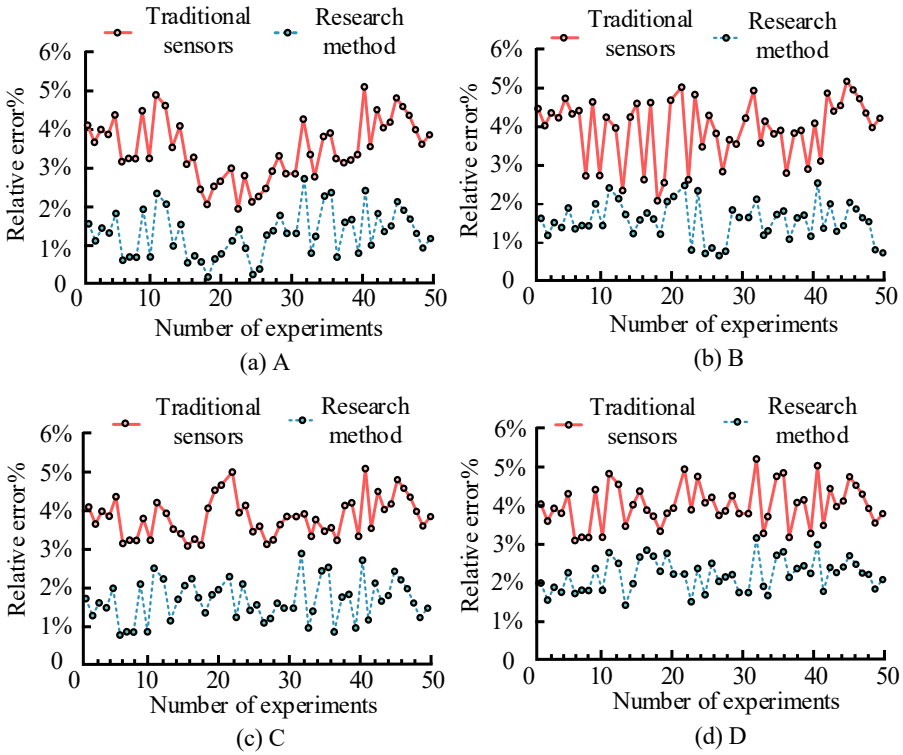


Fig. 3. Comparison of relative errors in sensor calibration between traditional sensors and research methods

To further validate the performance of this proposed algorithm, the root mean square error (RMSE) and SNR are compared with traditional wavelet threshold denoising, EEMD denoising, and improved wavelet lifting algorithm. This result shows that this proposed method has the smallest RMSE of 0.326 and the largest SNR of 11.3272. The larger value of SNR and the smaller RMSE indicate the better effect of noise cancellation.

Table 3

**Comparison of RMSE and SNR of several algorithms**

| Algorithm | Number of experimental samples | RMSE | SNR |
|---|---|---|---|
| Research method | 20 | 0.326 | 11.3272 |
| Traditional wavelet threshold denoising | 20 | 6.921 | 4.415 |
| EEMD denoising | 20 | 1.698 | 7.943 |
| Improved wavelet lifting algorithm | 20 | 2.618 | 9.932 |

The results of the experimental data of the robust correction model of this study are tabulated in Table 4. The robust correction model of the study shows significant results better. The mean of raw data fluctuates in the range of 8.97 to 15.32. After correction, the mean value is closer to the stable and reasonable range

(8.02~12.25). For example, in experiment 4, the original mean of 15.32 is reduced to 12.25 after correction, which effectively reduces the deviation of raw data. The standard deviation of raw data (1.89~3.56) reflects the high degree of data dispersion. The standard deviation of raw data (1.23~2.56) is significantly reduced after correction. It indicates that the model substantially suppresses the data fluctuation and improves the stability. Meanwhile, the mean (0.98~3.12) and standard deviation (0.65~1.56) of the error data are significantly reduced after correction, and the MAD (0.45~0.92) is also maintained at a low level. The robustness of the MAAD model in complex noise environments is fully verified, which can effectively correct the error and optimize the data quality. This provides a reliable correction scheme for signal processing of alternating current field sensors.

Table 4

**Table of experimental data results for robust calibration model**

| Experiment number | Mean of raw data | Standard deviation of raw data | Mean of error data | Standard deviation of error data | Mean of corrected data | Standard deviation of corrected data | Mean absolute deviation |
|---|---|---|---|---|---|---|---|
| 1 | 10.23 | 2.15 | 1 23 | 0.85 | 9.02 | 1.56 | 0.56 |
| 2 | 12.56 | 3.02 | 2.01 | 1.23 | 10.58 | 2.01 | 0.78 |
| 3 | 8.97 | 1.89 | 0.98 | 0.65 | 8.02 | 1.23 | 0.45 |
| 4 | 15.32 | 3.56 | 3.12 | 1.56 | 12.25 | 2.56 | 0.92 |
| 5 | 9.87 | 2.23 | 1.34 | 0.92 | 8.59 | 1.65 | 0.62 |

The Renyi entropy value is used in signal processing to measure the complexity of a signal and to determine whether it contains a large amount of random noise or complex patterns. Experiments are conducted to compare the Renyi entropy and reconstruction error of different non-smooth signal processing methods for alternating current field sensors. The comparison methods include Hilbert transform, multi resolution synchronous extraction transformation method, and traditional FT. The comparison results are shown in Fig. 4. In Fig. 4(a), the RMSE of the studied method is always kept at the lowest level during the iteration process. The RMSE between its reconstructed signal and the original signal is the smallest, converging at 0.326. The RMSEs of the other methods take values higher than 0.35, with slightly worse signal reconstruction accuracy. In Fig. 4(b), the research method also exhibits a lower Renyi entropy value, converging at 11.645. It shows that the method can better maintain the original information of the signal and reduce the loss of information when processing the signal.

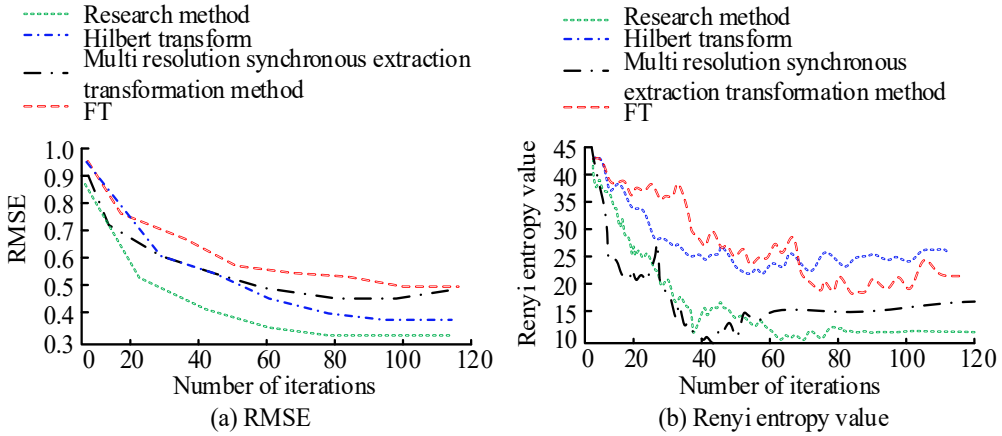


Fig. 4. Performance comparison of signal processing techniques for alternating current electric field sensors

## 4. Discussion and conclusion

A robust correction algorithm for the signal error of alternating current field sensors with JTFA was proposed. The algorithm was designed to extract the signal error features through JTFA, and adopt a robust correction model based on minimization MAD and adaptive TF window function. This realized the effective correction of the signal error in the complex noise environment. The experimental results indicated that the relative error of the traditional sensors fluctuated greatly and the mean value was high, while the error of the research method was more stable and had a small value. The relative error of traditional sensors fluctuated greatly in the range of 2%-6%. The mean of raw data fluctuated in the range of 8.97-15.32. After correction, the mean value was closer to the stable and reasonable range (8.02-12.25). The research method RMSE remained at the lowest level throughout the iteration process. Its RMSE between the reconstructed signal and the original signal was the smallest, converging at 0.326. The other methods took RMSE values higher than 0.35, with slightly poorer signal reconstruction accuracy. The research method also exhibited a lower Renyi entropy value, converging at 11.645. It indicated that the method could better maintain the original information of the signal and reduce the loss of information when processing the signal. In summary, the algorithm has high calibration accuracy and strong anti-interference ability. This provides a new solution for high accuracy measurement of alternating current field sensors.

**Fundings**

The research is supported by China Southern Power Grid Company Limited Science and Technology Project "Research and Application of Airborne Non-contact Multi-voltage Intelligent High-Voltage Detection Technology for Power Transmission and Transformation" (No. GDKJXM20231240).

## REFERENCES

[1] *B. Akbari, G. Sansavini,* Adaptive robust AC optimal power flow considering intrahour uncertainties, Electr. Power Syst. Res., Vol. **216**, Iss. 3, 2023.

[2] *G. Di Fresco, D. De Santis, C. Guarcello, B. Spagnolo, A. Carollo, D. Valenti,* Effects of correlated noise on the excitation of robust breathers in an ac-driven, lossy sine-Gordon system, Chaos Solitons Fractals, Vol. **189**, Iss. 1, 2024.

[3] *K. Ke, Q. Yang, J. Zhou, Z. Qiu, Z. Yao, N. Chen, W. Liao,* Piezoelectric PZT film-driven resonant torsional MEMS electric field sensor, IEEE Sens. J., Vol. **24**, Iss. 20, 2024.

[4] *J. A. Manzolli, J. P. F. Trovao, A. C. Henggeler,* Electric bus fleet charging management: A robust optimisation framework addressing battery ageing, time-of-use tariffs, and energy consumption uncertainty, Appl. Energy, Vol. **381**, Iss. 1, 2025.

[5] *J. Jiang, Q. Chen,* Universal and robust dynamic decoupling controls for zero-field magnetometry by using molecular clock sensors, Phys. Rev. A, Vol. **110**, Iss. 4, 2024.

[6] *F. Zare-Mirakabad, M. H. Kazemi, A. Doroudi,* Distributed robust control of frequency and active power-sharing ratio regulation in islanded AC microgrids. Electrical Engineering, 2024, 106(5): 5909-5918. DOI: 10.1007/s00202-024-02307-w.

[7] *A. Aff, M. Simab, M. Nafar, A. Mirzaee,* Robust linear parameter varying frequency control for islanded hybrid AC/DC microgrids, Electr. Power Syst. Res., Vol. **214**, Iss. 1, 2023.

[8] *A. Chen, F. Kopsaftopoulos, S. Mishra,* An unsupervised online anomaly detection method for metal additive manufacturing processes via a statistical time-frequency domain algorithm, Struct. Health Monit., Vol. **23**, Iss. 3, 2024.

[9] *A. C. Roque-Quispe, A. B. J. Alvarez-Quispe, P. R. Yanyachi, D. Yanyachi, J. C. Cutipa-Luque,* Robust control design on Scilab: Hybrid remotely operated vehicle, Comput. Appl. Eng. Education, Vol. **31**, Iss. 6, 2023.

[10] *X. Li, Y. Chen, H. Chen, R. Paul, X. Song, H. A. Mantooth,* A 10 kV SiC MOSFET power module with optimized system interface and electric field distribution, IEEE Trans. Power Electron., Vol. **39**, Iss. 8, 2024.

[11] *J. M. Warnecke, J. Lasenby, T. M. Deserno,* Author correction: Robust in-vehicle heartbeat detection using multimodal signal fusion, Sci. Rep., Vol. **14**, Iss. 1, 2024.

[12] *C. Liu, W. Xiang, H. Long, Y. Jia,* Spectral-efficient reference signal design and iterative channel estimation for OTFS modulation, IEEE Trans.Veh. Technol., Vol. **73**, Iss. 10, 2024.

[13] *Q. Peng, G. Yang, Q. Du,* Energy-saving optimization of frequency-variable heat pump air conditioning system for electric vehicles based on a genetic algorithm, Int. J. Autom. Technol., Vol. **24**, Iss. 6, 2023.

[14] *W. Jiang, J. Wang, P. S. Varbanov, Q. Yuan, Y. Chen, B. Wang, B. Yu,* Hybrid data-mechanism-driven model of the unsteady soil temperature field for long-buried crude oil pipelines with non-isothermal batch transportation, Energy, Vol. **292**, Iss. 1, 2024.

[15] *Kamalkant, P. Yadav, A. Ghosh, N. Singh, Shweta, H. Yadav, D. Singh, K. Singh, B. Santra,* Optimization of error signal lineshape for modulation-free robust laser frequency stabilization, Physica Scripta, Vol. **100**, Iss. 4, 2025.

[16] *Y. Kim, Y. K. Kim,* Physics-informed time-frequency fusion network with attention for noise-robust bearing fault diagnosis, IEEE Access, Vol. **12**, Iss. 1, 2024.
[17] *X. Q. Shang, L. Tang, T. L. Huang, N. B. Wang, W. X. Ren,* Time-varying characteristics analysis of bridge under moving vehicle using a modified time-frequency method with limited sensors, Eng. Struct., Vol. **316**, Iss. 1, 2024.
[18] *G. Wang, J. Wu, X. Chen, Y. Du,* A sensor signal processing method based on Hankel dynamic mode decomposition, Meas. Sci. Technol., Vol. **36**, Iss. 3, 2025.
[19] *Y. Zhou, W. K. Ling,* Local maximum-based synchroextracting transform with adaptive Time-varying parameter in the time-frequency chirp rate space, IEEE Tran. Instrum. Meas., Vol. **74**, Iss. 1, 2025.
[20] *C. Yang, L. Wang, C. Peng, S. Zhang, S. Cui, C. Ma,* A robust time-frequency synchronization method for underwater acoustic OFDM communication systems, IEEE Access, Vol. **12**, Iss. 1, 2024.
[21] *I. Ari,* A low carbon pathway for the turkish electricity generation sector, GLCE, Vol. **1**, Iss. 3, 2023.